

**5-Bit RF MEMS Phase Shifter Development in Ku Band  
for Phased Array Applications**

Submitted in partial fulfillment of the requirements

For the degree of

Doctor of Philosophy

By

**ANESH KUMAR SHARMA**

(Roll No: EE11P009)

Supervisors

Prof. SG SINGH

Prof. A DUTTA

Dr DVK Sastry



**Department of Electrical Engineering**

**INDIAN INSTITUTE OF TECHNOLOGY, HYDERABAD**

**2013**

## APPROVAL SHEET

Thesis titled "5-bit RF MEMS Phase Shifter Development in Ku Band for Phased Array Applications" IIT Hyderabad, Ph.D. Thesis Template by ANESH KUMAR SHARMA is approved for the degree of Doctor of Philosophy.



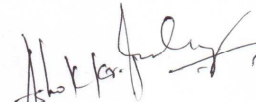
Examiners

Supervisors



Prof. S.G.SINGH

Prof. A DUTTA 

  
Observer

Date:

Place: Hyderabad

**INDIAN INSTITUTE OF TECHNOLOGY HYDERABAD,  
INDIA**

**CERTIFICATE OF COURSE WORK**

This is to certify that Mr. ANESH KUMAR SHARMA was admitted to the candidacy of the Ph.D. Degree in December 2010 and successfully completed all the courses required for the Ph.D. programme. The details of the course work done are given below.

---

<b>Sl. No.</b>	<b>Course No.</b>	<b>Course Name</b>	<b>Credits</b>
1	EE 5510	Analog IC Design	3
2	EE 6020	Wireless Sensor Networks	3
3	EE 5120	VLSI Technology	3
4	EE 5110	Device Physics & Modeling	3

---

Dy. Registrar (Academic)

IIT HYDERABAD

Dated:

Dedicated  
to  
My Parents

**Mrs. RAJ RANI SHARMA**

**Shri MAHENDRA SHARMA**

## Acknowledgements

Research and Development is a distinctive experience. I term it distinctive, since I come from the same back ground. My parent organization i.e. Research Centre Imarat, a part of Defence Research and Development Organization (DRDO) is a pioneer in the Defence R&D sector in our country. The trials and tribulations, the success and failures and the times of exhilaration and equanimity, a researcher experiences, have far reaching ramifications throughout life. It is a perennial process of learning, imparting the knowledge of handling situations, tackling problems and interacting with fellow humans. I must say I have learned a lot.

There has been help from many quarters. My first thanks are to my supervisors, Prof. Shiv Govind Singh, Prof. Asudeb Dutta and Dr DVK Sastry for their expert guidance and friendly care that guided me through the maze of RF MEMS and Micro engineering respectively. Though confronted with problems, more than I could handle, I sailed through under their able guidance.

I wish to thank my research progress committee members, Prof. Ashok Kumar Pandey, Prof. K Siva Kumar, Prof. Ketan P Detroja, Prof. Siva Rama Krishna, Ch. Sobhan Babu and Prof. CS Sharma for their valuable suggestions and encouragement during my research tenure. They have been extremely helpful and supportive throughout my research tenure.

I also wish to express my sincere thanks to all the faculty members in the IIT(H), especially Prof. UB Desai Director (IITH), Prof. Faiz Ahmed Khan Dean (Academics), Prof. Mohammed Zafar Ali Khan and Prof. P Rajalakshmi for their support and help.

I am thankful to the non-teaching staff of the Electrical Engineering department for their help on various occasions. I am also thankful to non teaching staff of IIT (H) especially to academic section for their kind help and cooperation.

I take this opportunity to express my sincere thanks to my senior colleagues Shri G Satheesh Reddy OS & Director RCI, Dr. SK Chaudhuri Former Director RCI, Dr CG Balaji Former Associate Director RCI, Shri M Ugender Reddy Sc‘G’ PD (MRSAM), Shri BRK Reddy Sc‘G’ APD (MRSAM), Shri JV Prasad Sc‘G’ Technology Director (DRS), and Shri N

Venkatesh Sc‘F’ RCI. Special thanks are due to my friends Ashu K Gautam and M Durga Prakash for their support and encouragement.

I am grateful to my brother Prof. Ashok Sharma for his constant inspiration during my research work. My special regards goes to my father in law Dr. JS Sharma and mother in law Smt. Pushpalata Sharma for their unconditional support and blessings.

Finally, I would like to thank my dear wife Mrs. Ritu Sharma for her loving and caring presence. Her calm and positive attitude always brings best out me even in dire conditions. She not only kept patience during all these years but also encouraged and supported me to achieve the best in academics. My daughter Vaishali and son Akshar & Aditya have been enthusiastic through my academic period.

Anesh Kumar Sharma

## ABSTRACT

MEMS based devices represent an extremely attractive alternative to MESFET devices for realization of the programmable phase shifters. The stable operation of RF MEMS devices is impacted by the actuation voltage, restoration force and the structural stresses. These can induce severe functional deformities into the device leading to operational problems. These parameters can be optimized by the concept of built-in reliability through design. In the present work, the study of Ku band 5-bit MEMS phase shifter was associated with the switch development. The hybrid design topology of switched and loaded line was adopted for the phase shifter. This topology has been the best trade off among large phase shift, low loss and reduced space requirement in the defined frequency band. This approach requires 18 switches per 5-bit phase shifter and all must work simultaneously in order to achieve the phase shifter fully functional. Hence the study was initiated with switch development keeping the focus on the above mentioned parameters.

The capacitive shunt and ohmic series switch were designed with a split beam concept which has been evolved uniquely in comparison to the holes commonly available in the literature. This has been implemented to overcome the various criticalities of restoration force and structural stress for stable operation and the advantage of the structure release due to large split area during the release process. In fact, it has been emphasised to achieve the higher spring constant with lower structural stress arising due to the structure design. A complete analysis of the spring constant and the stress was carried out to address the long term operation. In capacitive shunt type, two variations i.e. single and double dc bias was taken up for study. Both these configurations have been provided the symmetric actuation along the RF line for uniform pull-in. The configuration having single bias pad was conceived for simple implementation of the switch in the systems during practical application. Single DC bias pad has lot of ease in applying the DC potential in comparison to the two bias pad configurations however this needed to create a discontinuity in the RF line. The discontinuity has been provided in the single DC bias pad design. All other design parameters have been exactly same in both the configurations. Both the configurations have bias pad on the periphery so that smaller length of bond wire is sufficient during assembly and packaging to avoid the parasitic effects at high frequencies. The proposed split beam versus rectangular holes beam, most commonly exists in literature, analyzed with FEM (Coventorware simulator) for stress analysis. To observe the significance of split beam design

over rectangular holes type, beam surface area, thickness, material and mass were kept same. The analysis shows that the stress in case of rectangular holes is 630 MPa and 380 MPa for the split beam configuration about 35-40% lower. This analysis shows the superiority of split beam design with respect to the rectangular holes. The similar approach was followed for the ohmic series switch. In case of the cantilever the structural stress was found lower by 25-30% in comparison to the rectangular holes approach. The fabrication and characterization of these switches has shown the actuation voltage as 24.6V for capacitive shunt configurations. The RF parameters have been measured as insertion loss 0.20dB and 0.24dB, return loss 24.0dB and 22dB while isolation as 40dB and 37dB over 4-20 GHz frequency range for two dc bias pad and single bias pad configurations respectively. In case of the ohmic series switch the actuation voltage of 18.1V was achieved. The measurement has shown RF parameters as insertion loss 0.18dB, return loss 21dB and isolation better than 40dB over the DC-12GHz.

After developing a significant understanding, the study on the RF MEMS switches was extended to the design, simulation, fabrication and characterization of the 5-bit Ku band phase shifter. In the best of my knowledge this is first attempt to develop and implement a 5-bit MEMS based phase shifter in Ku band for the active phased array. This involves the singular bits, integrated 5-bit phase shifter on CPW configuration and microstrip version for implementation into the T/R module. The three bits namely  $180^\circ$ ,  $90^\circ$  and  $45^\circ$  have been designed using switched microstrip lines with series ohmic MEMS switches to achieve the large phase shift. The lower phase bits namely  $22.5^\circ$  and  $11.25^\circ$  have been designed using microstrip line sections loaded by ohmic MEMS switches in shunt mode. Microstrip topology additionally provides lower loss and enhanced compactness with respect to CPW. Electromechanical analysis of the MEMS parts of phase shifter has been carried out to optimize the critical parameters such as i) actuation voltage, ii) contact force due to series resistance and iii) deformation arising because of stress gradient. These have been studied in detail in order to ascertain the stable operation. The CPW version was characterized on-wafer using the TRL kit dedicatedly fabricated along with the devices. The measured RF results obtained for the monolithic 5-bit CPW MEMS phase shifter have been measured as the return loss better than 12dB and average insertion loss better than 3.21dB for the 32 states in the 16-18GHz frequency band. The minimum and maximum insertion loss was 2.15dB and 3.84dB respectively. The average return loss is 20.64dB. The average phase shift error has been 1.52 degrees. The worst case phase shift error was observed as 1.84 degrees over the 32 states.

Finally, our focus was on the microstrip version, and in order to evaluate the microstrip version, the control circuitry was developed to drive the phase shifter with the



programmable microcontroller for logic combination having the high voltage driver. The hardware has been provided an USB port to connect for PC interface to control the 12 dc signals necessary to drive the 5-bit phase shifter for 32 states measurement. The RF performance for the microstrip version has been measured as return loss better than 12.73dB and average insertion loss 4.68dB ( $IL_{\min} = 4.03\text{dB}$ ,  $IL_{\max}=5.17\text{dB}$ ) and the phase shift error (rms) for the 32 states is 2.83degrees. This insertion loss includes the loss towards the RF connectors and the test jig which is of the order of 1.35dB. The effective loss of the microstrip version phase shifter is 3.33dB for 5-bit phase shifter over 32 states in the 16-18GHz frequency band. These results have shown the potential of 5-bit Ku band MEMS phase shifter that can replace the MESFET based phase shifter in T/R module for AESA applications.

# CONTENTS

Approval Sheet	ii
Certificate of Course Work	iii
Acknowledgement	v
Abstract	vii
Contents	x
List of figures	xiv
List of tables	xxi
Abbreviations and Acronyms	xxii
References	140
List of Publication	152

## **Chapter 1 Introduction**

1.1	Motivation	1
1.2	Objectives of the thesis	4
1.3	Thesis Outline	5

## **Chapter 2 Literature Survey**

2.1	RF MEMS Switch – Brief Description and Fabrication	6
2.1.1	RF MEMS Switch-Technology Development	9
2.2	RF MEMS Phase Shifter	17
2.2.1	RF MEMS Phase Shifter Configurations	18
2.2.2	RF MEMS Phase Shifters- Technology development	20

## **Chapter 3 RF MEMS Switch Design Configurations & Simulation Results**

3.1	Design Topology for built-in reliability of different configurations	28
3.1.1	Design Flow	28
3.2	Design topology and Simulation	31
3.2.1	Split Beam Capacitive Shunt Configuration	31
3.2.2	Electromechanical Simulation Results	34
3.3	Layout Details	38
3.3.1	Double bias pad Configuration	38
3.3.2	Single bias pad Configuration	39
3.4	Simulation Results	40
3.5	Ohmic Series Configuration	41
3.5.1	Simulation Results	46

## **Chapter 4 Fabrication, Inspection & Measurement**

4.1	Process Flow	48
4.2	Inspection	50
4.2.1	Optical Inspection	50
4.2.2	Air gap measurement	50
4.2.3	Surface Topography Inspection	52
4.3	Experimental Results and Discussions	54
4.3.1	DC Characteristics	54
4.3.2	RF Characteristics	54
4.3.2.1	Double DC Bias Pad	55
4.3.2.2	Single DC Bias Pad	56
4.4	Fabrication – Ohmic Series	59
4.5	Inspection	59
4.5.1	Optical Inspection	59
4.5.2	Air gap measurement	60
4.5.3	Surface Topography Inspection	61
4.6	Experimental Results and Discussions	62
4.6.1	DC Characteristics	62
4.6.2	RF Characteristics	62

## **Chapter 5 Design & Simulation of 5 bit Ku band Phase Shifter**

5.1	Phase shifter design	66
5.2	RF Results of Ohmic Series Switch	67
5.3	Simulation Results of Single bits	68
5.4	5-bit Phase Shifter simulated performance	74
5.5	Layout of 5-bit phase shifter with CPW transition	74
5.6	Layout of Single bits & SPST for on wafer measurements	76
5.7	On-wafer TRL calibration kit	77
5.8	Layout of Microstrip configuration	78
5.9	Wafer level layout plan	78
5.9.1	Types of devices	78
5.9.2	Layout of devices on 4” mask	79
5.10	Analysis of MEMS structures	80

5.10.1	Equivalent Circuit	80
5.10.2	Electromechanical Analysis	80
5.11	Design of 5-bit switched line topology on GaAs	84
5.12	Integrated Phase shifter simulation Results	85
5.12.1	Simulation Results of Principal bits	86
5.12.1.1	11.25° Phase bit	86
5.12.1.2	22.5° Phase bit	87
5.12.1.3	45° Phase bit	87
5.12.1.4	90° Phase bit	88
5.12.1.5	180° Phase bit	89
5.12.2	Simulation Results of 5-bit Phase Shifter	90
5.12.2.1	Integrated 5-bit delay path results	90
5.12.2.2	Integrated 5-bit reference path results	91
5.13	Electromechanical Simulation	93
<b>Chapter 6 Fabrication and Process Inspection</b>		
6.1	Process Description	97
6.2	In-Process Inspection	104
6.3	Test Structure and Inspection Results	105
6.3.1	Spacers Thickness	105
6.3.2	Gold Thickness	106
6.3.3	Electrical Test Pattern	107
6.3.4	Electromechanical Test structure	108
6.3.5	SEM Inspection	109
<b>Chapter 7 On-Wafer RF Characterization of CPW Single bits and 5-bit Phase Shifter</b>		
7.1	Test set up and fabricated wafer layout	111
7.2	On-wafer TRL Calibration Kit	113
7.3	RF Performance of the Ohmic series SPST switch	114
7.4	Single Bit RF Performance	115
7.4.1	Measured results : 180° Phase bit 1	115
7.4.2	Measured results : 90° Phase bit 2	116
7.4.3	Measured results : 45° Phase bit 3	117
7.4.4	Measured results : 22.5° Phase bit 4	118

7.4.5	Measured results : 11.25° Phase bit 5	119
7.5	5-bit Phase shifter Measurements and Results	120
<b>Chapter 8 Microstrip Phase Shifter Characterization on Jig</b>		
8.1	MEMS Phase Shifter Test jig Design	124
8.2	Test Jig Description	128
8.3	Control Circuitry Description	129
8.4	Graphical User Interface	131
8.5	Hardware Setup	132
8.6	RF Characterization	133
<b>Chapter 9 Conclusion and Future Work</b>		
9.1	Conclusion	136
9.2	Future Scope of Work	139

## List of Figures

<b>Chapter</b>	<b>Titles</b>	<b>Page</b>
2.1	(a) Series Switch - Output is “High” when switch is closed, (b) Shunt Switch -Output is “Low” when switch is closed.	7
2.2	(a) and (b) shows the signal transmission flow of combined switches to achieve the high isolation	7
2.3	(a) the bulk micromachining (b) the surface micro machining	8
2.4	Raytheon capacitive shunt switch [44]	9
2.5	SEM View of the MEMS switch [45]	10
2.6	Low spring-constant MEMS switch [46]	10
2.7	LG-Korea high-capacitive-ratio MEMS shunt switch [49]	11
2.8	SEM view of DC-contact MEMS shunt switch of University of Illinois [51]	11
2.9	Berkeley see-saw series/shunt MEMS switch [54]	12
2.10	Switch from National Taiwan University using controlled residual stress [58]	13
2.11	Nanyang Technological University shunt switch in (a) single bridge (b) double bridge configuration[59].	13
2.12	SEM images of differnt configurations [61]	14
2.13	SEM image of the cantilever switch[62]	14
2.14	SEM image of top view of the switch [63]	15
2.15	Distributed transmission line digital phase shifter [72]	18
2.16	Configuration of the reflect line phase shifter [73]	19
2.17	Loaded line phase shifter configuration [74]	19
2.18	Switched line phase shifter configuration [76]	20
2.19	Raytheon phase shifter [79]	21
2.20	Rockwell DC-40 GHz switched line phase shifter [83]	22
2.21	Nanjing Institute phase shifter [85]	22
2.22	Image of the University of Perugia phase shifter [87]	23

2.23	Hybrid integrated 4-bit MEMS switched-line phase shifter [88]	23
2.24	SEM images of the fabricated V -band 2-bit phase shifter [92]	25
2.25	University of Michigan DMTL phase shifter [94]	25
2.26	SEM Image of the (a) fabricated phase shifter structure and (b) Cross section of the Membrane [95].	26
3.1	Flow for Design, Simulation and Device Development	29
3.2	(a) Cross section for shunt capacitive switch and (b) electrical equivalent	29
3.3	(a) Cross section for ohmic series switch and (b) electrical equivalent	30
3.4	(a) Top view of the two side bias pad and (b) shows single bias pad	31
3.5	Cross section of beam area with actuation pad	32
3.6	(a) and (b) Stress analysis 3D models for the split and rectangular holes beam respectively	33
3.7	Dimensions for the reduced model excluding anchors	34
3.8	Voltage versus displacement curve for pull-in	34
3.9	Contact and Hysteresis analysis curve	35
3.10	A 3D model of beam under pull-in and contact analysis	36
3.11	Transition analysis for ON/ OFF time	38
3.12	(a) Full view with dimensions, (b) Tapering, (c) Bias pad and (d) DC Line	38
3.13	(a) Full view with dimensions (b) RF line with discontinuity for dc bias provision, (c) electrodes view with dimensions (common for both configurations)	39
3.14	(a) and (c) Stress analysis whereas (b) and (d) shows the force versus displacement curve for split and rectangular holes cantilever respectively.	41
3.15	(a) Cross section for cantilever having actuation electrode, (b) and (c) shows the details of the first metal layer and of the actuation electrode respectively. All dimensions shown in figures are in $\mu\text{m}$ .	43
3.16	3D model of Cantilever under pull in analysis	44
3.17	Contact Analysis and Hysteresis curve	45
3.18	Switch Transition analysis for on / off time	46
4.1	(a) to (f) Cross section of fabrication flow followed during the switch fabrication	49
4.2	(a) Optical view of the fabricated double dc bias pad configuration,	50

	(b) Optical view of the fabricated single dc bias pad configuration	
4.3	Air gap measurement of beam from the bottom electrode in non contact mode using the laser vibrometer. The cantilever was scanned across the length so as to confirm the planarity. X and Y axis shows the width and length respectively. Z axis shows the gap height of the membrane from the bottom electrode.	51
4.4	(a) Scan direction and (b) Air gap was observed as 2.84 $\mu\text{m}$ from the top surface of the bottom electrode as against the Z axis.	52
4.5	(a) SEM view of the full device and (b) Zoomed SEM view of the membrane area of single dc bias pad	53
4.6	(a) SEM view of the full device and (b) Zoomed SEM view of the membrane area of double dc bias pad	53
4.7	Test set up for measurement of capacitance	54
4.8	Fabricated switch measurement set up for the CPW GSG configuration measured with 200 micron pitch probe for double DC bias.	55
4.9	S parameter measured results (a) upstate of the switch, return and insertion loss (ON state) and (b) downstate of the switch, isolation are compared against the simulated results (OFF state).	55-56
4.10	Fabricated switch measurement set up for the single bias pad configuration measured with 200 micron pitch probe.	56
4.11	S parameter measured results (a) upstate of the switch, return and insertion loss (ON state) and (b) downstate of the switch, isolation are compared against the simulated results (OFF state).	57
4.12	Cross section of the ohmic series switch	59
4.13	Optical view of ohmic series configuration	59
4.14	Air gap measurement of cantilever from the bottom electrode in non contact mode using the laser vibrometer. The cantilever was scanned across the length so as to confirm the planarity. X and Y axis shows the width and length respectively. Z axis shows the gap height of the cantilever as 2.9 $\mu\text{m}$ from the bottom electrode.	60
4.15	(a) SEM view of the complete series switch and (b) Zoomed SEM view Cantilever area	61
4.16	Fabricated switch measurement set up showing the CPW	62



4.17	(a) S parameter results in upstate of the switch. Measured results of the return loss and isolation are compared against the simulated results (OFF state).	63
	(b) S parameter results in downstate of the switch. Measured results of the return and insertion loss are compared against the simulated results (ON state).	
5.1	Layout (a) and expected performance (b) of the MEMS SPST cantilever switch constituting the phase shifter	68
5.2	(a) Layout, (b) simulated return loss, (c) insertion loss and (d) phase shift of 180° bit '1'.	69
5.3	(a) Layout, (b) simulated return loss, (c) insertion loss and (d) phase shift of 90° bit '2'.	70
5.4	(a) Layout, (b) simulated return loss, (c) insertion loss and (d) phase shift of 45° bit '3'.	71
5.5	(a) Layout, (b) simulated return loss, (c) insertion loss and (d) phase shift of 22.5° bit '4'.	72
5.6	(a) Layout, (b) simulated return loss, (c) insertion loss and (d) phase shift of 11.25° bit '5'.	73
5.7	Simulated performance for (a) return loss, (b) insertion loss and (c) phase shift of the 5-bit MEMS phase shifter for all 32 states.	74
5.8	Layout of the 5 Bit MEMS Phase shifter with CPW transition.	75
5.9	(a) Zoomed view of a DC pad including dimensions. All DC pads have identical dimensions, (b) zoomed view of the line of DC pads in the upper part of the die. The pitch between pads is constant and equal to 0.6mm. The line in the bottom part of the die is identical to the one in the upper part. Microstrip and Coplanar versions are based on identical DC Pad dimensions, position and pitch. (c) Zoom on the CPW to Microstrip via-less interconnection.	76
5.10	Layout of single bits including CPW transition and Ohmic series switch for on-wafer measurement.	77
5.11	(a) TRL calibration kit layout and (b) LINE simulated return loss.	77
5.12	Layout of the 5-bit microstrip MEMS phase shifter.	78
5.13	Complete 4" mask layout of the phase shifter.	79

5.14	(a) Layout and (b) simplified equivalent circuit of the Series Ohmic cantilever MEMS Switch.	80
5.15	(a) Layout and (b) simplified equivalent circuit of the Series Ohmic cantilever MEMS Switch.	81
5.16	Tip bending versus the stress gradient for different spring lengths $l_s$ .	82
5.17	Cantilever stiffness as a function of the stress gradient for different spring lengths $l_s = 10, 20, 30$ and $40 \mu\text{m}$ .	82
5.18	(a) Layout and definitions (b) analysis in case of zero stress gradient and (c) analysis in case of $15\text{MPa}/\mu\text{m}$ stress gradient.	83
5.19	Individual 5-bit layout for fabrication on GaAs.	85
5.20	(a) MWO image and (b) Insertion and Return loss for $11.25^\circ$ bit1.	86
5.21	(a) MWO image and (b) Insertion and Return loss for $22.5^\circ$ bit2.	87
5.22	(a) MWO image and (b) Insertion and Return loss for $45^\circ$ bit3.	88
5.23	(a) MWO image and (b) Insertion and Return loss for $90^\circ$ bit4.	89
5.24	(a) MWO image and (b) Insertion and Return loss for $180^\circ$ bit5.	90
5.25	a) MWO image, (b) Insertion and Return loss and (c) Phase for 5-bit delay path.	91
5.26	(a) MWO image and (b) Insertion and Return loss and (c) Phase for 5-bit reference path.	92
5.27	Integrated layout of the 5-bit Phase Shifter on GaAs.	93
5.28	(a) Cross sectional view, (b) top view and (c) 3D view of the switch part	93-94
5.29	Pull-in point, Contact and Hysteresis Analysis curve	95
6.1	a) Thermal oxidation; poly-silicon, TEOS deposition and contact opening, b) metal deposition and patterning. The images display the view after the poly and the metal etch.	99
	(c): LTO deposition, via opening and floating metal deposition. The images shows the via etch and the floating metal etch.	100
	(d): Spacer deposition and backing. The Image shows the spacer image after the fabrication step.	101
	(e): Seed layer and first Au/Bridge" electroplating and the Image of the bridge deposition is shown.	102
	(f): Second Au /CPW electroplating and release of suspended structures. The Image shows the die with zoomed view of the CPW Deposition,	103

	final Pre-release and final structure.	
6.2	Scheme of the test structures across the wafer with the position of parametric test pattern (red squares), thickness test pattern (blue squares) and electromechanical test structures (yellow squares).	105
6.3	Spacer thickness profile on device wafer. Nominal value = 3000 nm.	106
6.4	Test pattern for gold thickness measurement of the BRIDGE (pale yellow -1), CPW (gold-yellow - 2) and BRIDGE+CPW (brown -3) gold layers.	106
6.5	Electrical Test Pattern.	107
6.6	Electromechanical Test Structure pattern.	109
6.7	(a) and (b) Complete view of the 11.25° and 22.5° bit respectively while (c) shows the Zoomed view of cantilever part and the (d) zoomed view of different layers.	109-110
7.1	Test Setup for on wafer probe characterization of single bits and phase shifter with CPW interconnections	112
7.2	(a) Partial layout and (b) part of the fabricated wafer.	112
7.3	(a) Image of TRL calibration kit with reference planes (red dot line), and (b) LINE measured Return Loss and Insertion Loss.	113
7.4	(a) Image of MEMS SPST cantilever in series with a 1.8mm long coplanar line and (b) measured isolation at 0V in comparison with the ideal switch (switch actuated by design).	114
7.5	(a) Image and layout, (b) measured phase shift, (c) return loss and (d) insertion loss of Bit 1 (180 degrees).	115
7.6	(a) Image and layout, (b) measured phase shift, (c) return loss and (d) insertion loss of Bit 2 (90 degrees).	116
7.7	(a) Image and layout, (b) measured phase shift, (c) return loss and (d) insertion loss of Bit 3 (45 degrees).	117
7.8	(a) Image and layout, (b) measured phase shift, (c) return loss and (d) insertion loss of Bit 4 (22.5 degrees).	118
7.9	(a) Image and layout, (b) measured phase shift, (c) return loss and (d) insertion loss of Bit 5 (11.25 degrees).	119
7.10	Image of fabricated phase shifter with an example of the polarization on dc bias pads of the device to achieve the Phase shift of 292.5°.	121

7.11	An example of binary format (10 10 01 11 00), (Phase shift= $180^\circ + 90^\circ + 22.5^\circ = 292.5^\circ$ ).	122
7.12	Measured performance of the 5-bit MEMS phase shifter for 32 states (a) output return loss, (b) input return loss, (c) insertion loss and (d) Phase shift.	122
8.1	Test jig design (a) SMA connectors and (b) end launch connectors.	125
8.2	Microstrip layout of test jig version.	125
8.3	Interface of the die with bond wire and substrate details.	126
8.4	RF performances of the (a) non-compensated structure and (b) the compensated structure with the L-C section and the multiple bond wires.	126-127
8.5	(a) RT duroid layout and its connectorized version while (b) shows the RF insertion loss of test jig over 0-40GHz frequency range.	127
8.6	Image of the fabricated microstrip version.	128
8.7	(a) and (b) dc interconnections along with die, (c) FR4 cap and (d) the final view after assembly	129
8.8	(a) Control board with its principal parts and (b) the mounting scheme of the assembled phase shifter on to the control board.	130
8.9	(a) Switches combination and the $V_{out}$ generated the DIP switch. (b) Zoom on the High Voltage Test Point to be used to verify the actual voltage value.	131
8.10	The Graphic User Interface.	132
8.11	Test set up configuration of microstrip phase shifter.	133
8.12	Image of the physical set up of microstrip phase shifter.	133
8.13	Shows measured performances of the 5-bit MEMS phase shifter, (b, and c) Output/Input return loss, (d) Insertion loss, and (e) phase measured over 32 states.	134

## List of Tables

2.1	Comparison of RF MEMS Phase Shifters performance of different groups	27
3.1	Dimensional details for the membrane	33
3.2	Modal Analysis For Resonance Frequency	37
3.3	Simulation Results – Split Beam Capacitive Switch	40
3.4	Modal Analysis frequency for Cantilever	45
3.5	Summary of Simulation results for Ohmic series configuration	46
4.1	Summary of Parameters for the developed Shunt Switch	58
4.2	Summary of Parameters for The developed Ohmic Switch	64
5.1	Type and number of all of devices incorporated in the wafer layout	79
5.2	Modal Analysis for Resonance Frequency	95
5.3	Summary of 5-bit Phase Shifter	96
6.1	Parameters measured on the Test Wafers of the Batch	104
6.2	Spacer Thickness. All values in $\mu\text{m}$	106
6.3	Gold layer thickness values for BRIDGE, CPW and BRIDGE + CPW. All values in microns.	107
6.4	Measured Electrical Test Parameter presented with the Mean Values	108
7.1	On-wafer measurements for $180^\circ$ phase bit 1	115
7.2	On-wafer measurements for $90^\circ$ phase bit 2	116
7.3	On-wafer measurements for $45^\circ$ phase bit 3	117
7.4	On-wafer measurements for $22.5^\circ$ phase bit 4	118
7.5	On-wafer measurements for $11.25^\circ$ phase bit 5	119
7.6	Summary of the achieved phase error of the individual phase bits	120

## ABBREVIATIONS and ACRONYMS

Symbol	Description	Unit
k	Spring constant	N/m <sup>2</sup>
d	gap between electrodes	μm
A	Area of electrode	μm <sup>2</sup>
ε	permittivity of air	F/m
t	Thickness of membrane	μm
E	Young's Modulus	GPa
W	width of the beam	μm
t <sub>ε</sub>	Switching Time	μsec
V <sub>p</sub>	pull in voltage	Volts
V <sub>s</sub>	source voltage	Volts
f <sub>o</sub>	resonant frequency	KHz
V	applied voltage	Volt
x	displacement	μm
v	poisson's ratio	--
C <sub>up</sub>	Upstate capacitance	fF
C <sub>down</sub>	Downstate capacitance	pF
ΔΦ	Differential phase shift	degrees
Φ <sub>2</sub>	Phase of delay path	degrees
Φ <sub>1</sub>	Phase of reference path	degrees
S <sub>21</sub>	insertion loss	dB
S <sub>11</sub>	return loss	dB

### Abbreviations:

AESA	Active Electronically Steerable Antennas
PESA	Passive Electronically Steerable Antennas
RF	Radio Frequency
IC	Integrated Circuit
MMIC	Monolithic Microwave Integrated Circuit

EW	Electronic Warfare
MEMS	Micro Electro Mechanical Systems
MESFET	Metal Semiconductor Field effect transistor
T/R	Transmit/ Receive
GaAs	Gallium Arsenide
CPW	Coplanar Waveguide
PECVD	Plasma Enhanced Chemical Vapor Deposition
SEM	Scanning Electron Microscope
SOLT	Short Open Load Thru
SPST	Single Pole Single Throw
TRL	Thru Reflect Line
LPCVD	Low Pressure Chemical Vapor Deposition
DC	Direct current